

PAPER

Correlated vibrations in ion-pair dynamics in mechanoactivation identify functional domains of force-dependent titin kinase†

Cite this: *Soft Matter*, 2013, **9**, 9897

Ming-Chya Wu,^{*ab} Jeffrey G. Forbes^{‡c} and Kuan Wang^{*bcd}

Titin kinase is a mechanoenzyme, whose activity is activated by mechanical stretching and binding of calcium sensors. Stretching causes local and global conformational changes of secondary structures and complex movements of ion pairs and transient formations of salt bridges. This paper applies the adaptive time series analysis approach to study the mechanical responses of ion-pair movements to stretch unfolding through steered molecular dynamics (SMD) simulations, focusing on the ion-pair dynamics of mechanoactivation obtained from the SMD trajectories. Temporal correlation analysis of the ion-pair time series shows that the activation process involves changes of secondary structure. Spectral analysis defined several groups and subgroups of the ion pairs with vibrational damping/resonance in the scale of ~ 0.5 Å, corresponding to vibrational modes of chemical bonds. Examination of these groups revealed the locations or neighboring structures of the autoinhibitory loop, ATP binding cleft, catalytic loop, and P+1 loop, all key functional domains of this kinase. We propose that the correlated vibrations of subgroups of ion pairs have significant correlations with functional domains, which can be used to identify, *a priori*, special functional and structural features of folded proteins.

Received 3rd June 2013

Accepted 21st August 2013

DOI: 10.1039/c3sm51539g

www.rsc.org/softmatter

Introduction

Protein folding/unfolding is an important biological process and has attracted major research interest in biophysical communities for more than a half century. Protein unfolding processes induced by chemicals, acids, and more recently mechanical force allow us to probe unfolding transition states in detail, useful for understanding interactions in the molecules. Among these, mechanically induced unfolding is interesting because the signature of individual unfolding intermediates in the force–extension profile represents structural properties, manifesting the energy landscape of the protein.¹ Unfolding intermediates of proteins are experimentally accessible by a variety of single molecule manipulation approaches, such as atomic force microscopy (AFM)² and optical tweezers.^{3,4} However, such techniques usually operate in a time

scale of 10^{-3} s, which is much slower than the typical oscillatory frequency of molecules in the time scale of 10^{-9} to 10^{-12} s. Detailed structures of the unfolding characters are thus still unavailable experimentally due to the limited resolution. In such cases, numerical simulation such as molecular dynamics (MD) is a powerful tool to gain insights at the desired high time and atomic resolution.

In this paper, we apply an adaptive time series analysis approach to study the ion-pair dynamics in the force-induced unfolding of human titin kinase simulated by steered molecular dynamics (SMD). Titin kinase is a 321 amino acid residue (Fig. 1 (a)) mechanoenzyme located near the C-terminus of the giant (3–4 MDa) elastic protein titin⁵ that spans 1/2 of the contractile machinery (sarcomere) in skeletal and cardiac muscles.⁶ Titin is pivotal in force generation, sensing and transduction in skeletal and cardiac muscles. The reversible extension of titin generates passive tension, and the activity of titin kinase is modulated by mechanical stretching, thereby transducing the mechanical signals to biochemical pathways in regulating the assembly and turnover of the sarcomeres. *In vivo*, it is inhibited by a C-terminal regulatory (inhibitory) tail which blocks the ATP binding site and by tyrosine phosphorylation in the active site. It is activated, under mechanical stretching, when tyrosine phosphorylation releases inhibition by the P+1 loop.^{7,8} The molecular mechanism of this novel force sensitive kinase is being pursued by experimental and theoretical studies of enzymology, mechanical unfolding of single molecules by AFM and SMD simulations.⁸ Remarkably, the success of SMD

^{*}Research Center for Adaptive Data Analysis, National Central University, Chungli 32001, Taiwan. E-mail: mcwu@ncu.edu.tw

^bInstitute of Physics, Academia Sinica, Nankang, Taipei 11529, Taiwan

^cMuscle Proteomics and Nanotechnology Section, Laboratory of Muscle Biology, National Institute of Arthritis and Musculoskeletal and Skin Diseases, National Institutes of Health, Bethesda, Maryland 20892, USA

^dNanomedicine Program, Institute of Biological Chemistry, Academia Sinica, Nankang, Taipei 11529, Taiwan

† Electronic supplementary information (ESI) available: See DOI: 10.1039/c3sm51539g

‡ Present address: TWIC, Inc, 4423 Lehigh Road, #172, College Park, MD 20740, USA.

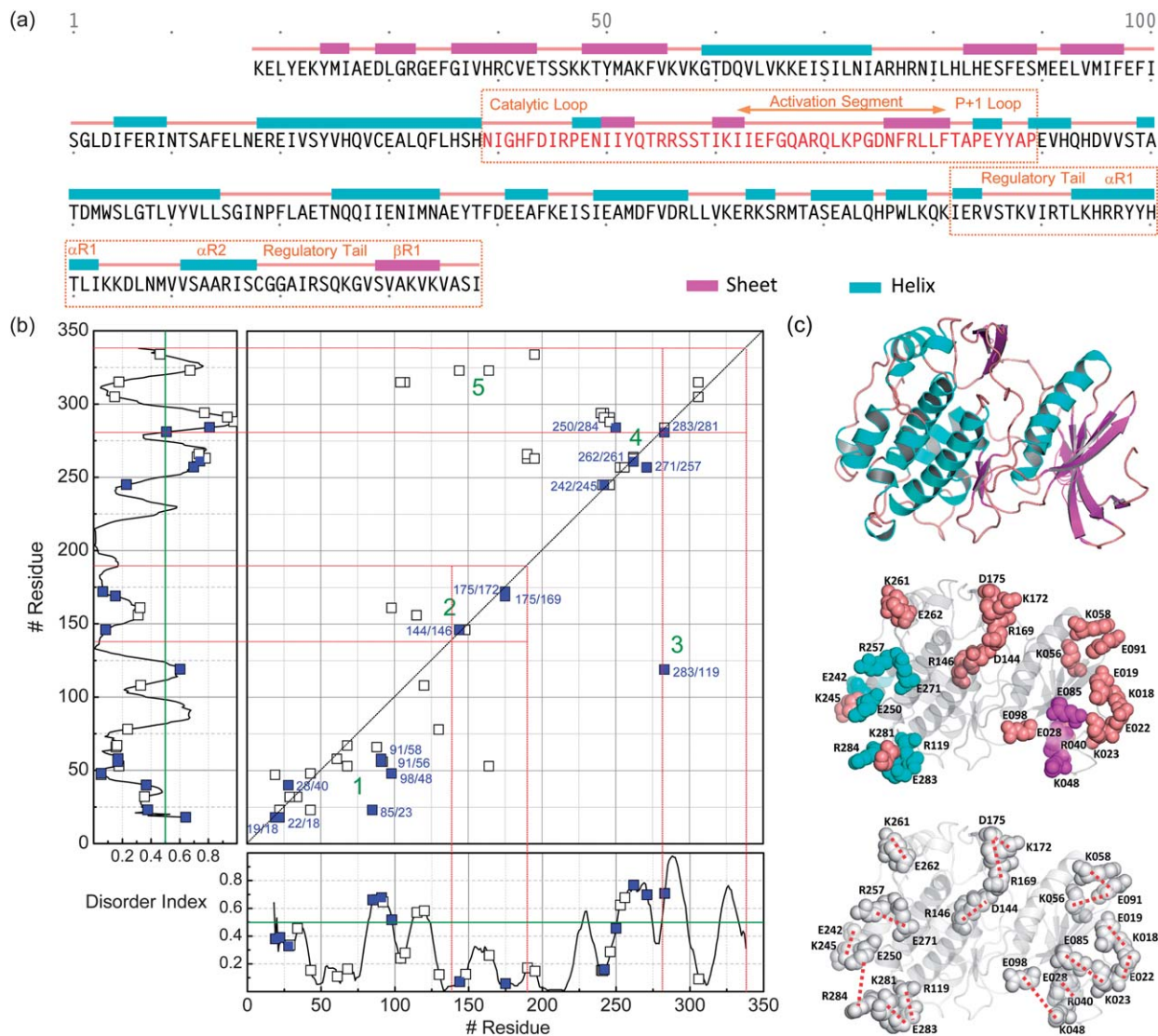


Fig. 1 Ion pairs and disorderness profile of the titin kinase domain. (a) Sequence and secondary structures of titin kinase. The active-site region (residues 138–189) and regulatory tail (282–338) are highlighted by the boxes. (b) Diagonal map of all ion pairs (\square) and those with explicit oscillations of frequency 0.11×10^9 Hz in their time series (\blacksquare). The disorder index is calculated by PONDR (<http://www.pondr.com/>) using a VL-XT predictor. A larger index value corresponds to a lower probability of a fixed tertiary structure. (c) The structure of titin kinase (PDB code: 1TKI) (top), relative locations of the residues (middle) and the corresponding ion pairs (bottom).

simulations has been demonstrated by single-molecule experiments *in vitro* and *in silico*.^{9–12} For titin kinase, it suggested atomic details of sequential domain unfolding accompanying the activation process,⁸ suitable for identifying changes that contribute to the activation process. The dynamics of ion pairs and salt-bridges are likely important in understanding the complex global structural response of protein toward mechanical stress. A network of salt-bridges has been shown to play a role in the small scale conformational transition during the activation of the Src family of tyrosine kinases.¹³ We initiate, to our knowledge, the first analysis of the network of electrostatic interactions of titin kinase through the unfolding process.

A salt-bridge is a combination of non-covalent interactions of hydrogen bonding and electrostatic interactions. It arises from a pair of oppositely charged residues, including aspartic acid or glutamic acid with arginine, lysine, or histidine.¹⁴ The distance and orientation between the residues participating in the salt-

bridge are crucial; those ion-pairs with separations greater than the cut-off are not qualified as a salt-bridge.^{15,16} The salt-bridges are among the most thoroughly investigated interactions in protein chemistry due to their important and specific functions.¹⁷ They serve as binding sites in enzymes,^{18–20} mediate molecular recognition,^{21–23} and modulate the allosteric behavior of proteins.^{24,25} Recently, it has been shown that salt-bridges can be sensitive drug targets in nucleoproteins to inhibit viral replication.²⁶

The SMD simulates the extension and unfolding of single protein molecules with a constant velocity or force by controlling the end-to-end distance. Since the SMD simulations record coordinates of all atoms in the system at all time points, all atomic interactions are defined. These simulations of the stretching of titin kinase allow the changes in all ionic and non-ionic interactions to be monitored over the course of the simulation. Interestingly the possible salt-bridges form and

break as the molecule is stretched as inspected visually. To understand the dynamics of the ionic interactions as well as the formation and breakage of salt-bridges, we carried out the SMD simulations with different pulling speeds and analyzed the SMD trajectories using time series analysis approaches, with the aim of defining the most critical set of a global network of molecular interactions that underlie force generating/bearing events, and detect essential components in an ion-pair time series which reflect significant nanomechanics in activation processes.

Materials and methods

Steered molecular dynamics simulations

We used the NAMD package^{27,28} with the CHARMM22 force field²⁹ and CMAP corrections³⁰ to implement the simulations. The SMD method involves the application of external forces to molecules in MD simulations. The simulations started from an X-ray structure, deposited as entry 1TKI⁷ in the Protein Data Bank.³¹ The amino acid residues are numbered from 18 to 338 (numbering from N to C terminus). (Our numbering system follows the numbering in the PDB entry 1TKI. In some references, such as ref. 32, the numbering of the residues is renumbered from 1 to 321.) All structural models were visualized and manipulated with VMD.³³ The C_α of the N-terminal residue was first positioned to the origin of the coordinate system. The protein model was then rotated to position the C_α of the C-terminal residue on the x-axis, and solvated with an 8 Å TIP3P model water³⁴ shell with the Solvate program.³⁵ VMD was used to add water molecules to render a water box of size 200 Å × 84 Å × 80 Å to allow for the stretched molecule to remain surrounded by water at all times. Ions (K⁺ and Cl⁻) were added to the hydrated structures to an ionic strength of 150 mM using the Meadionize Plugin,³⁶ which places ions at the minima of the electrostatic potential map generated by the Potential utility of the MEAD program suite.³⁷ Finally, the system contained 142 948 atoms.

Following minimization, the system was warmed to 300 K in 6 K steps with 500 steps of MD at each temperature increment. After reaching 300 K, an additional 50 000 steps of MD were performed to further equilibrate the system. All MD simulations were done at a 1 fs step size with particle mesh Ewald (PME) calculation of long-range electrostatic interactions. The density of grid points for PME was $\sim 1 \text{ \AA}^{-3}$. Nonbonded interactions were calculated at every step and full electrostatic interactions were calculated at every other step. The simulations were performed with a uniform dielectric constant of 1, and a cut-off of Coulomb forces with a switching function starting at a distance of 8 Å and reaching zero at 12 Å. SMD simulations were carried out by fixing the N-terminus of the domain, and applying an external force to pull a restraint point (residue) of the C-terminus with a constant velocity in the direction along the vector from the fixed atom (C_α 18, N-terminus) to pulled atom (C_α 338, C-terminus). The forces experienced by the C_α atom of a pulled residue are

$$f = k(vt - y) \quad (1)$$

Here y is the displacement of the pulled atom from its original position, and k is the spring constant. Referring to the parameters justified in ref. 32, here the value of k was set at 1 kcal mol⁻¹ Å⁻², corresponding to 69.48 pN Å⁻¹. The force-induced unfolding was simulated with the pulling speed in a range from $v = 0.005 \text{ \AA ps}^{-1}$ to $v = 0.05 \text{ \AA ps}^{-1}$, including 2 realizations with $v = 0.005 \text{ \AA ps}^{-1}$, 2 realizations with $v = 0.01 \text{ \AA ps}^{-1}$, and 1 realization with $v = 0.05 \text{ \AA ps}^{-1}$. Fig. 2 shows a typical force curve of the force-induced unfolding of titin kinase simulated by 25 000 ps SMD with pulling speed $v = 0.005 \text{ \AA ps}^{-1}$, and the corresponding snapshots taken at $t = 0$, 9998, and 25 000 ps. At 9998 ps, significant structural changes such as the loss of helicity in α R2 of the regulatory tail already occurred. It should be noted that the calculated paths of unfolding of titin kinase can be influenced by the specific protocol applied.³⁸ The present study follows with interest certain unfolding events associated with significant structural changes, and the kinase is not necessarily fully activated. To avoid confusion, in the following, our demonstration in the main text will be based on this realization. The analysis of the other realizations with the same and different pulling speeds is presented in the ESI.[†]

Ion-pair and salt-bridge time series

The salt-bridges in titin kinase were defined by an oxygen-nitrogen distance cut-off of any ion pair. An ion pair is considered as a salt-bridge as the separation of its oxygen-nitrogen pair is within the cut-off in at least one frame in the trajectory of unfolding. The cut-off is usually set to 4 Å; yet we follow the setting in VMD³³ and chose 3.2 Å as the cut-off. The time evolution of these ion pairs was calculated throughout the SMD trajectories. The number of ion pairs is realization dependent. In the typical realization of the simulation with pulling speed $v = 0.005 \text{ \AA ps}^{-1}$, there are 55 ion pairs involved in the unfolding of titin kinase. For other cases, there are 66 ($v = 0.005 \text{ \AA ps}^{-1}$), 63 ($v = 0.01 \text{ \AA ps}^{-1}$), 82 ($v = 0.01 \text{ \AA ps}^{-1}$), and 41 ($v = 0.05 \text{ \AA ps}^{-1}$) ion pairs (see ESI[†] for details). For the current case, the amino acid residues involved in the ion pairs and their topological locations are shown in Fig. 1. Here we are particularly interested in the simulation of the first 11 112 ps (11 113 data points), in which the system is not stretched too much to lose its main structure and the biological activity is activated from the structure change in the regulatory tail^{8,32} (see Fig. 2). We use a one-letter symbol and three digits to indicate an amino acid residue and its location in a linear sequence. Thus, notation E068 indicates the glutamic acid at position 68. Fig. 3(a) shows typical data of the ion pair (E068-K067) in the unfolding simulation of titin kinase. These data record the dynamic breaking and rejoining of salt-bridge during unfolding. To explore properties of the ion-pair time series, we define the gain $g_\tau(t)$ of $x(t)$,

$$g_\tau(t) = \frac{x(t + \tau) - x(t)}{x(t)}, \quad (2)$$

where τ is a multiple of the primary time sampling unit Δt (=1 ps). The gain time series $g_1(t)$ for the data of Fig. 3(a) is shown in

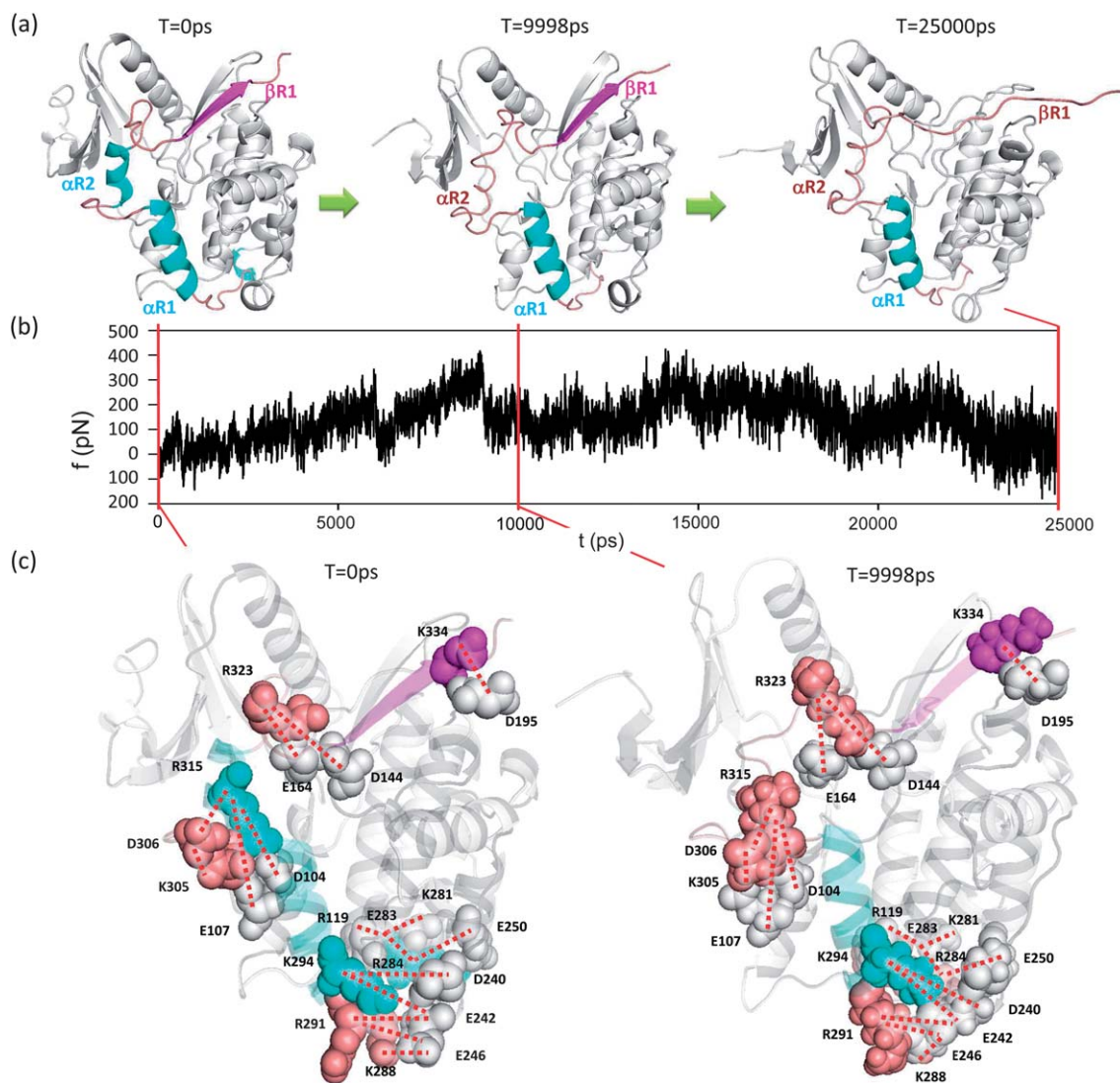


Fig. 2 Force-induced structural unfolding of titin kinase SMD simulation with pulling speed $0.005 \text{ \AA ps}^{-1}$. (a) Key force-induced unfolding events on the helical structures $\alpha R1$ and $\alpha R2$ (blue), and β sheet structure $\beta R1$ (magenta) that occurred at $t = 0, 9998$, and $25\ 000$ ps. (b) A typical force–extension curve. (c) Some of the ion-pair networks at $t = 0$ ps and $t = 9998$ ps. Ion pairs of increasing complexity, with two, three, four and eleven ions are shown. Note the changes in the relative orientation and spacing as the kinase is stretched.

Fig. 3(b). The probability density functions (PDFs) $P(g_\tau(t))$ for the gain $g_\tau(t)$ with time scales $\tau = 1, 4, 16$, and 64 are shown in Fig. 3(b). The distribution is non-Gaussian type, with fat tails. Further, the distribution of $P(g_\tau = 0)$ with respect to τ in the logarithmic scale is linear (see Fig. 3(c)).^{39–42} The best fitting straight line is, with a stability index $\beta \approx 5$,

$$\log_{10} P(g_\tau = 0) = C - \frac{1}{\beta} \log_{10} \tau, \quad (3)$$

where C is a constant. This suggests that the fluctuation of the ion-pair distance is generated by a random multiplicative process with finite variance. Infrequent but large changes in the distance occur as parts of the structures unfold, resulting in the fat tails in the PDF. There is a probability for the existence of temporal correlation in ion-pair dynamics, which can be studied by scaling analysis. In the following, we focused on the data of $g_{\tau=1}(t)$.

Temporal correlation analysis

The detrended fluctuation analysis (DFA)⁴³ is used to assess the temporal correlation of the ion-pair time series. We first constructed a gain walk $w(t)$ by accumulating $g_{\tau=1}(t)$ according to $w(t) = \sum_{t'=t_0}^t g_{\tau=1}(t')$. The DFA is an analysis based on the measurement of fluctuations F of the time series $w(t)$ in different scales. The algorithm of DFA is given by:⁴³

$$F(n) = \sqrt{\frac{1}{T} \sum_{t=1}^T [w(t) - w_n(t)]^2} \propto n^\alpha, \quad (4)$$

where n is a scale factor for resampling $w(t)$, and $w_n(t)$ is the straight line with the slope determined by the best fitting of the data points of $w(t)$ in the moving window of size n . The slope for the curve in the plot of F as a function of n in the log–log scale is

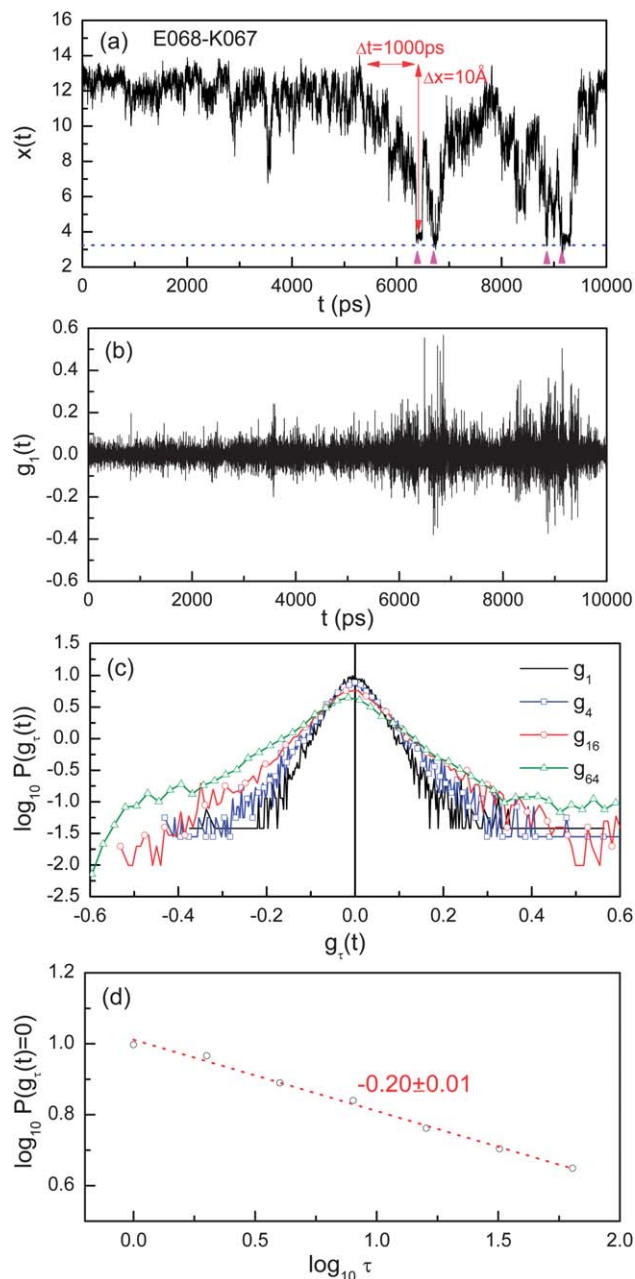


Fig. 3 Stability analysis of ion-pair data. (a) Ion-pair time series E068-K067. The blue (dotted line) indicates the salt-bridge cut-off of 3.2 Å. Pink triangles indicate formation of salt-bridges. (b) The corresponding gain $g_i(t)$. (c) The probability distribution of gain $g_i(t)$ defined in (2) with $\tau = 1, 4, 16$, and 64. (d) Probability of gain variations $P(g_i(t) = 0)$ as a function of the time sampling intervals τ . The slope of the best-fit straight line is -0.20 ± 0.01 .

associated with the intrinsic correlation of the time series, characterized by the index α .⁴³

Hilbert spectral analysis

To examine the existence of oscillatory features associated with dynamic breaking and rejoining, we analyze the frequency content of the ion-pair time series. Since the time series is highly nonstationary and nonlinear, to achieve high resolution to detect the oscillation, we used the empirical mode

decomposition (EMD) to decompose each ion-pair time series into a number of intrinsic mode functions (IMFs) and then analyzed the corresponding Hilbert spectrum and power spectral density (PSD). The decomposition is achieved by iterative “sifting” processes for extracting modes by identification of local extremes and subtraction of local means.^{44–49} The iterations are terminated by a criterion of convergence. For the details of the algorithms of EMD, reference is made to ref. 44 and 45. For an ion-pair time series $x(t)$, we have

$$x(t) = \sum_{k=1}^n c_k(t) + r_n(t), \quad (5)$$

where $c_k(t)$'s are IMFs, and $r_n(t)$ is a residue, usually a monotonic trend. The Hilbert transform is performed on each IMF according to

$$c_k(t) + i\bar{c}_k(t) = A_k(t)e^{i\phi_k(t)}, \quad (6)$$

where $\bar{c}_k(t)$ is the conjugate of the IMF $c_k(t)$, calculated from

$$\bar{c}_k(t) = \frac{1}{\pi} P \int_{-\infty}^{\infty} \frac{c_k(t')}{t-t'} dt', \quad (7)$$

where P indicates the Cauchy principle value; $A_k(t) = \sqrt{c_k^2(t) + \bar{c}_k^2(t)}$ is the amplitude, and $\phi_k(t) = \tanh^{-1}[\bar{c}_k(t)/c_k(t)]$ is the instantaneous phase. The instantaneous frequency is calculated by taking the time derivative of $\phi_k(t)$. The decomposition satisfies completeness and orthogonality.⁴⁴ The orthogonality index, $\kappa = \sum_{i,t} c_i(t)c_{i+1}(t) / \sqrt{\sum_{i,t} c_i^2(t) \sum_{j,t} c_{j+1}^2(t)}$, was used to choose a reasonable decomposition by minimizing the value of κ . The mode mixing problem is processed by using ensemble empirical mode decomposition (EEMD),⁵⁰ which is an extended version of EMD. Different sifting criteria were used in EEMD to confirm the robustness of the decomposition.

Results and discussions

Temporal correlation in ion-pair dynamics

An example DFA analysis for ion pair E068-K067 is shown in Fig. 4(a). There are two characteristics of the time series in short and long time scales, contributing to the *linear* parts in the two regimes. In short-time scales less than 50 ps, there is anti-persistent behavior such that $\alpha_1 = 1.11$, while persistent behavior dominates in time scales larger than 100 ps, with $\alpha_2 = 1.83$. The distributions of α_1 and α_2 for all 55 time series are shown in Fig. 4(b). On average, $\langle \alpha_1 \rangle = 1.16$ and $\langle \alpha_2 \rangle = 1.81$. Specifically, in short time scales, the variations of the ion-pair distance are associated with thermal fluctuations. It shares similar properties of Brownian motion with $\alpha = 1$. For long time scales from 100 ps to 3000 ps, a rough estimate based on the change of interionic distance from 13.2 Å at $t = 5400$ ps to 3.2 Å at $t = 6400$ ps (*i.e.*, velocity $\Delta x/\Delta t \sim 0.01$ Å ps⁻¹) in Fig. 3(a) suggests that the corresponding length scale is in a range from 1 to 30 Å. Since amino acids have an average radius of 3.5 Å,⁵¹ this length scale is the same as one to ten amino acid residues. The

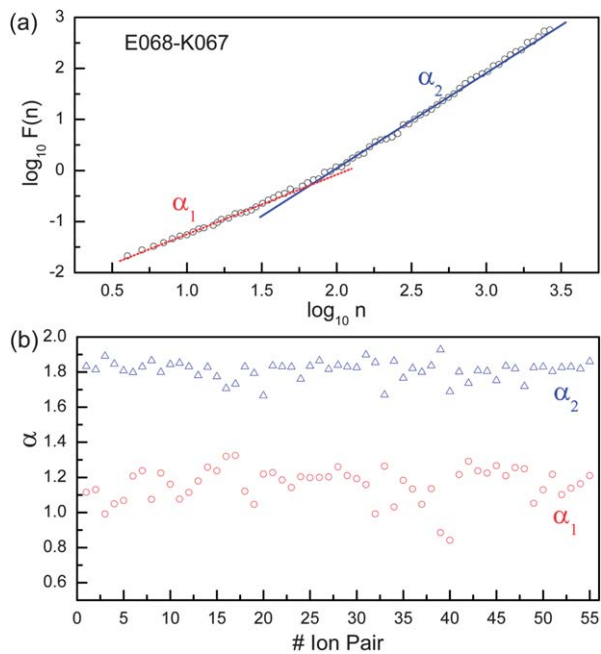


Fig. 4 Scaling analysis of an ion-pair time series. (a) Log–log plot of $F(n)$ as a function of n , for E068-K067. The slopes determined by linear fittings are $\alpha_1 = 1.11$ and $\alpha_2 = 1.83$. (b) Distribution of the α values of the 55 ion pairs.

variations of the ion-pair distances in this time scale reflect the unfolding, mainly of secondary structures. These observations are valid also for force-induced unfolding in different pulling-speeds (see ESI[†]), in which the α values do not vary significantly.

Hilbert spectra of ion-pair time series

A typical decomposition of ion-pair time series E283-R119 (Fig. 5(a)) is shown in Fig. 5(b), and the corresponding PSD is shown in Fig. 5(c). This ion pair, between the regulatory tail and the adjoining region of the active site, forms a salt-bridge that breaks, rejoins, and breaks (see Fig. 5(a)), related to the force events at $t = 4000$ and 6000 ps in the force curve of Fig. 2(b). From Fig. 5(b), we visually searched oscillatory behaviors in various time scales and noted that c_{13} is of special interest in this case. The IMF c_{13} has an oscillation with the frequency of 0.11×10^9 Hz and a decaying amplitude. This oscillation contributes to the peak in the PSD of Fig. 5(c). It is worth emphasizing that such an oscillation cannot be observed directly from the ion-pair time series in Fig. 5(a). It suggests the existence of a mechanical damping mechanism for this ion pair in response to stress. The amplitude of the vibrational damping is in the scale of ~ 0.5 Å, corresponding to vibrational modes of chemical bonds. A similar oscillation has been observed for other ion pairs, mainly located at the boundary surface of C- and N-lobes, and at the junction between them. Table 1 presents the ion pairs with explicit oscillations by bold font. Their topological locations are shown in Fig. 1(b) and (c). Note that similar oscillatory behaviors have been observed in other realizations of different pulling speeds (see ESI[†]), while the characteristic frequency varies. This suggests that the vibrational damping is a general feature for the force-induced unfolding of titin kinase.

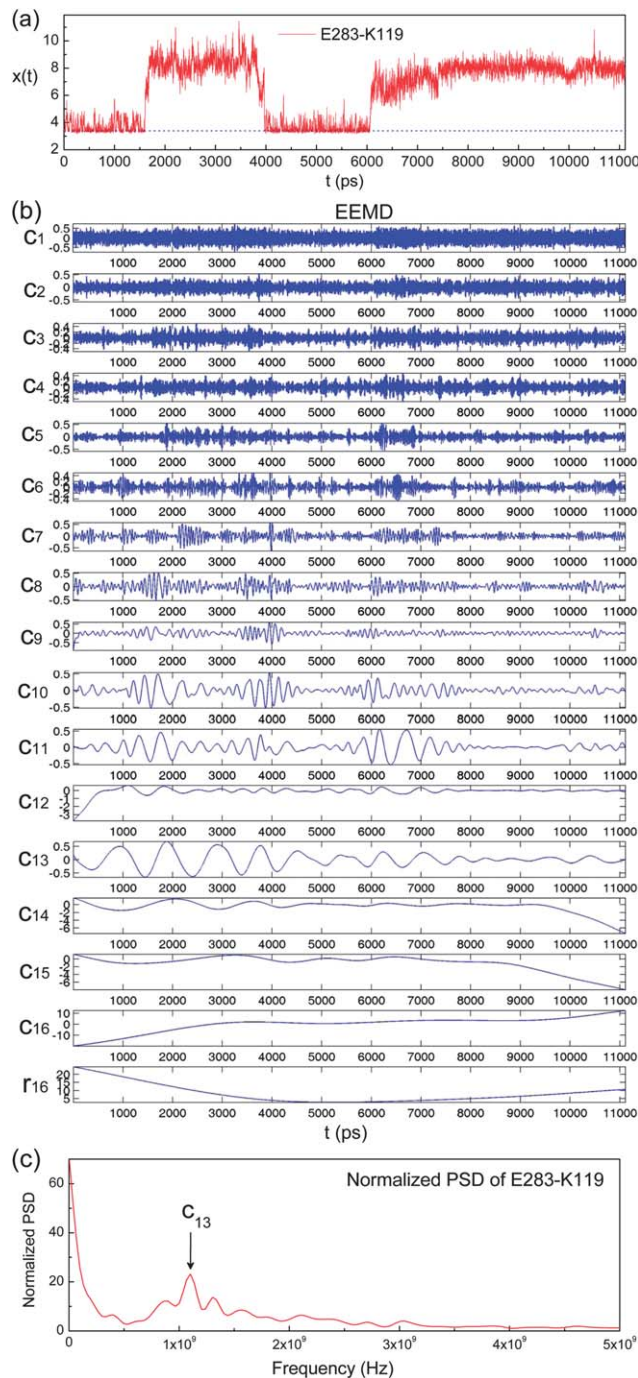


Fig. 5 Hilbert spectral analysis of an ion-pair time series. (a) Ion-pair time series E283-K119. The blue (dotted) line indicates the salt-bridge cut-off of 3.2 Å. (b) The ensemble empirical mode decomposition (EEMD). (c) The corresponding power spectral density (PSD).

We have found that typical oscillations in the ion-pair time series are mainly of relatively lower frequency in the order of 10^9 Hz. This corresponds to a period of several hundred ps, or several Å in length scale (with the velocity of 0.01 Å ps^{-1} , estimated from Fig. 3(a)), essentially the scale associated with a typical secondary structure. Additional examples of distinct oscillatory behaviors for three ion pairs with 10^9 Hz frequency oscillation (E283-R119, E085-K023, and D144-R146) and three

Table 1 Classification of ion pairs. Groups 1, 2, ..., 5 are classified by topological locations in a linear sequence (see Fig. 1(b)) and their subgroups (I, I*, ...) are classified by the existence of explicit oscillation. Salt-bridges in unstretched protein are underlined. Salt-bridges formed during stretch are without underline. The ion-pair time series having explicit oscillatory behaviors at a frequency of about 0.11×10^9 Hz are further highlighted by bold font

| Group | Subgroup | Ion pairs |
|-------|----------|---|
| 1 | I* | E028-R040, E019-K018, E022-K018, E085-K023, E091-K056, E091-K058, E098-K048 |
| | I | <u>E088-K066</u> , E019-K047, E022-K023, D029-R032, E034-R032, E043-K023, E092-K056, E120-R108, E043-K048, D061-K058, E068-K053, E068-K067, E130-R078, E164-K053 |
| 2 | II* | D144-R146, D175-R169, D175-K172 |
| | II | <u>E098-K161</u> , E148-R146, E115-R156 |
| 3 | III* | E283-R119 |
| 4 | IV* | E242-K245, E250-R284, E262-K261, E271-R257, E283-K281 |
| | IV | E190-R263, D240-K294, E246-R291, D253-R257, E190-R266, D195-R263, E241-K245, E242-R291, E242-K294, E246-K245, E246-K288, D256-R257, E262-R263, E262-K264, E283-R284, D306-K305, D306-R315 |
| 5 | V | D104-R315, E107-R315, D144-R323, E164-R323, D195-K334 |

ion pairs without this frequency oscillation or with a higher frequency oscillation $\sim 10^{10}$ Hz (E190-R266, D144-R323, and E107-R315), and the IMFs c_{13} of each time series are shown in Fig. 6(a)–(f). Significant changes in the interionic distance (mostly corresponding to formation/breaking/rejoining of salt-bridges when the distance reduces to 3.2 Å) are marked in the $x(t)$ time series with triangles. It is apparent that the oscillatory behavior is a manifestation of significant changes in the interionic distance. The amplitude of oscillation appears to decrease and increase with the formation and breakage of salt-bridges, respectively. For the ion pair E283-K119, the breakage of salt-bridge at 1600 ps led to an increase in amplitude and the rejoining at 4000 ps caused an attenuation of the amplitude and then an increase when it breaks near 6000 ps. Similar behaviors are apparent for other ion pairs (such as E085-K023). This correlation is illustrated by the stable salt-bridges E190-R266 (Fig. 6(d)) and E107-R315 (Fig. 6(f)) where occasional breakages lead to large amplitude oscillation transiently from the stable non-oscillatory baselines. Sudden changes in the ion-pair distance, even without salt-bridge formation/breakage, are sufficient to attenuate or increase the amplitude. This is illustrated in the behaviors of E085-K023 between 6500 ps and 9300 ps, for D144-R146 (Fig. 6(b)) between 2000 ps and 5000 ps and for D144-R323 (Fig. 6(e)). There is a wealth of mechanical features in the oscillatory analysis of ion-pair distances, including evidence of harmonic damping and resonance (*e.g.* in E085-K023) that reflects the energy transfers from and to these networked ion pairs. Since the amplitudes of both harmonic damping and resonance are in the scale of vibrational modes of chemical bonds, we speculate that such oscillations may be detectable by Raman spectroscopy.⁵² A more thorough analysis is in progress.

Ion-pair dynamics and structural correlation

To assess the structural basis of the grouping of ion-pair dynamics during mechanical stretching, we plotted the two oscillation groupings of 55 ion pairs on the titin kinase secondary structures as well as the disorderness profile along the primary sequence (Fig. 1(b)) of titin kinase. The disorderness profile is defined by the disorder index, in which a larger index value corresponds to a lower probability of fixed tertiary structures. The intrinsically disordered protein regions display rapid conversion of transient secondary structures and unstructured coils and therefore are of particular interest from the angle of elasticity and force bearing/generating events. We used several predictors to assess the order/disorder profile of the titin kinase domain. The order/disorder profile displaying the relative propensity of disorderness based on the VL-XT predictor of PONDR^{53–55} (<http://www.pondr.com/>) is shown in Fig. 1(b). The locations of the 55 ion pairs on the primary sequence as well on the disorder profile are depicted topologically as five groups (1, 2, ..., 5) from the N- to C-terminus: ion pairs with the explicit oscillation as four subgroups: I* (E019-K018, E022-K018, E028-R040, E091-K058, E085-K023, E098-K048, and E091-K056), II* (D175-K172, D144-R146, and D175-R169), III* (E283-R119), and group IV* (E242-K245, E250-R284, E262-K261, E271-R257, and E283-K281) and the ion pairs without the explicit oscillation as four subgroups: I, II, IV, and V. Except groups 3 and 5, the other groups are distributed near the diagonal line indicating ion pairs formed from nearby side chains on the primary sequence. The general feature is that ion pairs in groups 3 and 4 located at the C-terminus are mostly bridging disorder/disorder regions. The ion-pairs of this kind form transient salt-bridges during stretching, as illustrated by the time series of E283-K119 in Fig. 6(a). The group 1 ion pairs near the N-terminus are mostly disorder/order combinations, which form transient salt-bridges more frequently, as illustrated by the pair E085-K023 in Fig. 6(b). The group 2 ion pairs are order/order combinations, with oscillations that are damped quickly, as illustrated by D144-R146 in Fig. 6(c). Compared with disorder/disorder and disorder/order combinations, the ion-pairs from the order/order combination appear to facilitate the rejoining of salt-bridges. The most striking behaviors are for the ion pairs in group V depicting the ion-pair dynamics of the regulatory tail. All pairs are order/disorder combinations from more distant amino acids in the primary sequence and, interestingly, all without any significant low frequency vibrations (see *e.g.*, Fig. 6(e) and (f)). Among the five realizations we simulated, the only one exception to this observation is a realization with pulling speed $v = 0.01 \text{ \AA ps}^{-1}$ (see Fig. 2(b) of ESI†), where an ion-pair E118-K288 in group 5 (V*) shows oscillatory behaviors. However, it is at the boundary of the regulatory tail. These observations suggest that the ion pairs in the regulatory tail act as a group in resisting conformational changes as titin kinase is stretched and undergo force-induced activation.

To understand further the structural features associated with the groups of vibrational correlated ion pairs and the corresponding physical significance, we examined their locations, their corresponding mechanical properties, and the functional

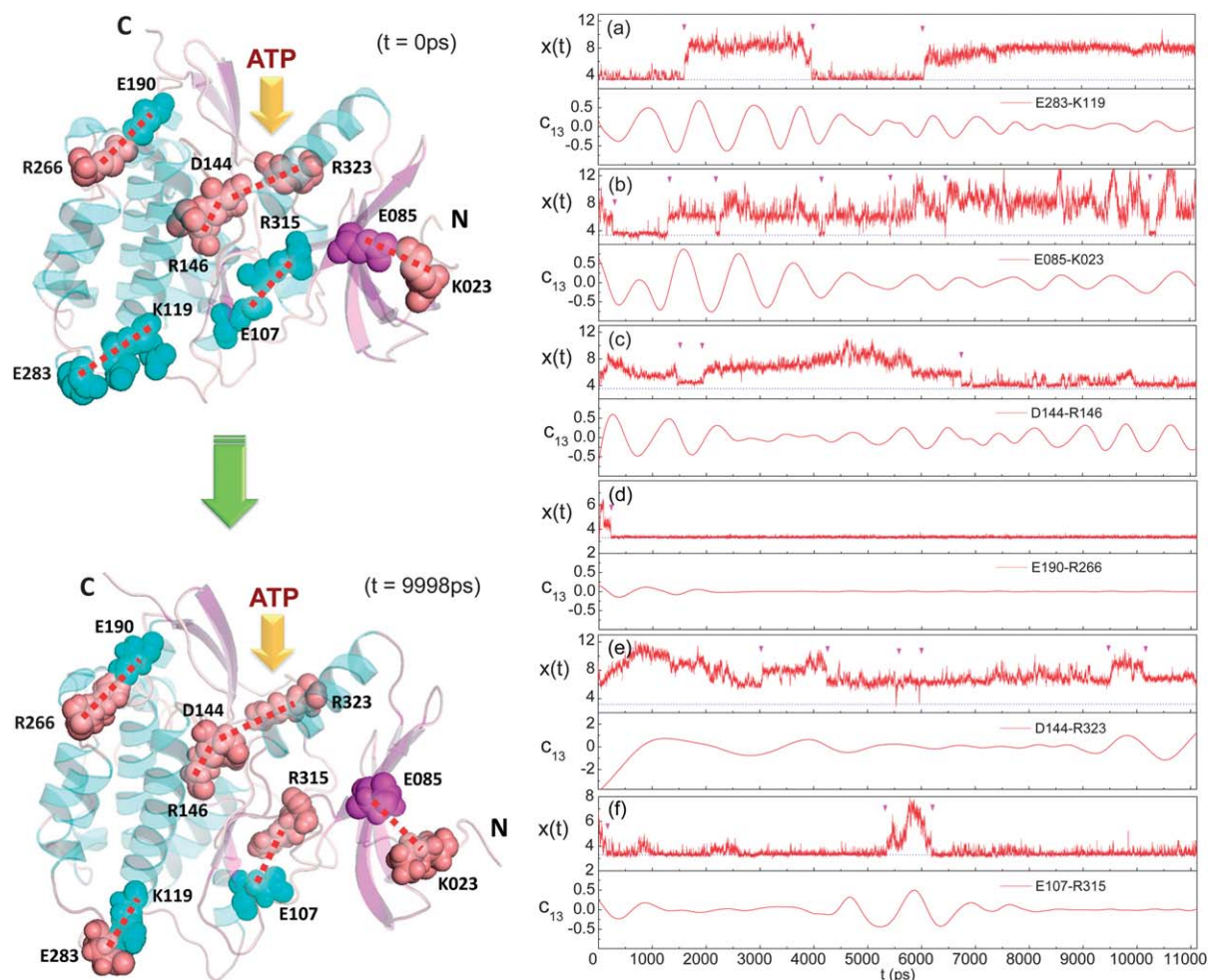


Fig. 6 Topological locations of ion pairs with and without dominant frequency at 0.11×10^9 Hz. Left: schematic of titin kinase and the residues in the ion pairs E283-R119, E085-K023, D144-R146, E190-R266, D144-R323, and E107-R315, at $t = 0$ ps (top) and at $t = 9998$ ps (bottom). Right: the ion-pair time series $x(t)$ and the IMFs c_{13} of (a) E283-R119, (b) E085-K023, (c) D144-R146, (d) E190-R266, (e) D144-R323 and (f) E107-R315. The blue (dotted) line indicates the salt-bridge cut-off of 3.2 Å. Pink down-triangles indicate significant changes in the interionic distance.

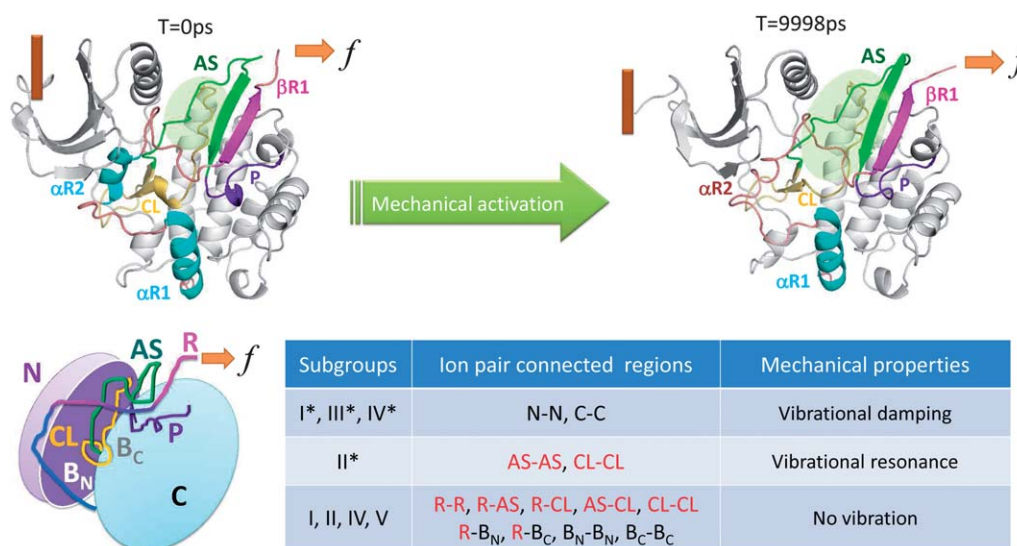


Fig. 7 Grouping of vibration-correlated ion pairs in the time series of unfolding intermediates of titin kinase upon stretching. The groups with the explicit oscillation (I*, II*, III*, and IV*) and the group without the explicit oscillation (I, II, IV, and V), the corresponding ion-pair connected regions, and mechanical properties of the ion-pair time series are depicted. The structure of titin kinase is illustrated as two half spheres labeled with N and C. Boundaries of the two spheres are denoted as B_N and B_C. Functional domains significant for kinase activity are abbreviated as: activation segment (AS), Catalytic loop (CL), P+1 loop (P), and Regulatory tail (R), and are represented in red font in the table.

domains of titin kinase, shown in Fig. 7. Since titin kinase is activated when the P+1 loop initially blocking the catalytic loop is removed,^{7,32} we noted, from Fig. 1(a) and Table 1, that there are 8 ion pairs involved in the active site consisting of three segments: catalytic loop (CL), activation segment (AS), and P+1 loop (PL). They were classified into different groups: E164-053 (AS-CL, subgroup I in Table 1), E148-R146 (CL-CL, subgroup II), D144-R323 (CL-R, subgroup V), D175-K172 (AS-AS, subgroup II*), D144-R146 (CL-CL, subgroup II*), E164-R323 (AS-R, subgroup V), E115-R156 (N-CL, subgroup II) and D175-R169 (AS-AS, subgroup II*); here “R” was used to indicate regulatory tail and “N” was used to indicate the segment of N-lobes. Except E148-R146, which is a salt-bridge in the unstretched protein and is without explicit oscillation, the ion pairs formed by the residues from the same segments form salt-bridges during stretching and are with explicit oscillation. There are no ion pairs formed by the residues from the P+1 loop. As the active site has a relatively ordered profile (see Fig. 1(b)), we speculate that the vibrational resonance in D175-K172, D144-R146, and D175-R169 is essential to the conformation adjustment, and the incollective behaviors (*i.e.*, classification in different groups) increase the efficiency. The absence of ion pairs in the P+1 loop likely makes it easy to be removed under stretching.

Conclusion

In summary, we have applied adaptive time series analysis approaches to investigate the ion-pair dynamics in the force-induced unfolding of titin kinase through SMD simulations. By studying the SMD trajectories during the activation by the structural changes in the regulatory tail, we defined an ion-pair time series which manifests properties of dynamic breaking and rejoining of the salt-bridges. The temporal properties were analyzed by scaling analysis of DFA, which revealed an anti-persistent behavior in short-time scales less than 50 ps, and a persistent behavior in long time scales greater than 100 ps. The former is attributed to thermal fluctuation, while the latter is likely associated with interactions involving secondary structures, implying that the activation process involves changes of secondary structures. Spectral analysis based on the EMD method shows that there is a characteristic oscillation with amplitude in the scale of vibrational modes of chemical bonds in some ion-pair time series. The ion pairs with such an oscillation are relatively active components, working as vibrational damping machinery to consume mechanical energy of stretching, and as vibrational resonance for conformation adjustment. Examination of the structural location of the groups of vibrational correlated ion pairs revealed the locations or neighboring structures of key functional domains of titin kinase, including the autoinhibitory loop, ATP binding cleft, catalytic loop, and P+1 loop. Furthermore, our analysis suggests that the ion pairs in the regulatory tail act as a group in resisting conformational changes as titin kinase is stretched and undergoes force-induced activation. Remarkably, the conclusions hold for different realizations with various pulling speeds in SMD simulations.

Our analysis of the time series of mechanically unfolded intermediates pays special attention to the correlated vibrations of chemical bonds from the oscillatory modes in the ion-pair time series. The structural features of correlated vibration reveal the functional domains of titin kinase in the stretch-activation process, as well as the role of intrinsically disordered domains of titin kinase in energy transduction during mechanical unfolding. To our knowledge, this represents the first successful attempt to unravel the meaning of the intricate kinetic and time dependent events during mechanical unfolding of proteins at atomic resolution. While we focus in the present study on titin kinase to investigate the force-induced structural and activity changes of this mechanoenzyme, our systematic time series analysis is applicable to any particular group of atoms such as hydrophobic, hydrophilic, and hydrogen bonding amino acids in any type of protein, both globular and intrinsically disordered. The potential application of our algorithms for identifying key functional and kinetic events that underlie structural transitions and activities is well worth exploring.

Acknowledgements

This work was supported by the National Science Council of the Republic of China (Taiwan) under Grant no. NSC 96-2112-M-008-021-MY3, 97-2627-B-008-004, and 100-2112-M-008-003-MY3, NCTS of Taiwan, and the Nanomedicine Program of Academia Sinica. This work was also supported in part by the Intramural Research Program of the National Institute of Arthritis and Musculoskeletal and Skin Diseases, NIH, DHHS. This study utilized the high performance computational capabilities of the Biowulf PC/Linux cluster at NIH (<http://biowulf.nih.gov>). NAMD was developed by the Theoretical and Computational Biophysics Group in the Beckman Institute for Advanced Science and Technology at the University of Illinois at Urbana-Champaign.

References

- 1 C. Jarzynski, *Phys. Rev. Lett.*, 1997, **78**, 2690–2693.
- 2 M. Rief, M. Gautel, F. Oesterhelt, J. M. Fernandez and H. E. Gaub, *Science*, 1997, **276**, 1109–1112.
- 3 M. Kellermayer, S. Smith, H. Granzier and C. Bustamante, *Science*, 1997, **276**, 1112–1116.
- 4 L. Tskhovrebova, J. Trinick, J. Sleep and R. Simmons, *Nature*, 1997, **387**, 308–312.
- 5 K. Wang, J. McClure and A. Tu, *Proc. Natl. Acad. Sci. U. S. A.*, 1979, **76**, 3698–3702.
- 6 K. Wang, R. McCarter, J. Wright, J. Beverly and R. Ramirez-Mitchell, *Biophys. J.*, 1993, **64**, 1161–1177.
- 7 O. Mayans, P. F. M. van der Ven, M. Wilm, A. Mues, P. Young, D. O. Furst, M. Wilmanns and M. Gautel, *Nature*, 1998, **395**, 863–869.
- 8 E. M. Puchner, A. Alexandrovich, A. L. Kho, U. Hensen, L. V. Schäfer, B. Brandmeier, F. Gräter, H. Grubmüller, H. E. Gaub and M. Gautel, *Proc. Natl. Acad. Sci. U. S. A.*, 2008, **105**, 13385–13390.
- 9 M. Sotomayor and K. Schulten, *Science*, 2007, **316**, 1144–1148.

- 10 M. Sotomayor and K. Schulten, *Biophys. J.*, 2008, **94**, 4621–4633.
- 11 E. H. Lee, J. Hsin, M. Sotomayor, G. Comellas and K. Schulten, *Structure*, 2009, **17**, 1295–1306.
- 12 J. Oroz, A. Valbuena, A. M. Vera, J. Mendieta, P. Gomez-Puertas and M. Carrion-Vazquez, *J. Biol. Chem.*, 2011, **286**, 9405–9418.
- 13 E. Ozkirimli and C. B. Post, *Protein Sci.*, 2006, **15**, 1051–1062.
- 14 D. A. Dougherty, *Modern Physical Organic Chemistry*, University Science Books, 2006.
- 15 S. Kumar and R. Nussinov, *J. Mol. Biol.*, 1999, **293**, 1241–1255.
- 16 S. Kumar and R. Nussinov, *ChemBioChem*, 2002, **3**, 604–617.
- 17 D. J. Barlow and J. M. Thornton, *J. Mol. Biol.*, 1983, **168**, 867–885.
- 18 J. F. Riordan, K. D. McElvany and C. L. Borders, *Science*, 1977, **195**, 884–885.
- 19 J. F. Kirsch, G. Eichele, G. C. Ford, M. G. Vincent, J. N. Jansonius, H. Gehring and P. Christen, *J. Mol. Biol.*, 1984, **174**, 497–525.
- 20 J. Singh, J. M. Thornton, M. Snarey and S. F. Campbell, *FEBS Lett.*, 1987, **224**, 161–171; Erratum in *FEBS Lett.*, 1988, **228**, 357.
- 21 J. Tormo, D. Blaas, N. R. Parry, D. Rowlands, D. Stuart and I. Fita, *EMBO J.*, 1994, **13**, 2247–2256.
- 22 B. E. Raumann, M. A. Rould, C. O. Pabo and R. T. Sauer, *Nature*, 1994, **367**, 754–757.
- 23 B. M. Brown, M. E. Milla, T. L. Smith and R. T. Sauer, *Nature Struct. Biol.*, 1994, **1**, 164–168.
- 24 M. F. Perutz, *Q. Rev. Biophys.*, 1989, **22**, 139–236.
- 25 T. E. Schirmer and P. R. Evans, *Nature*, 1990, **343**, 140–145.
- 26 Y.-F. Shen, Y.-H. Chena, S.-Y. Chu, M.-I. Lin, H.-T. Hsu, P.-Y. Wu, C.-J. Wu, H.-W. Liu, F.-Y. Lin, G. Lin, P.-H. Hsu, A.-S. Yang, Y. S. E. Cheng, Y. T. Wu, C. H. Wong and M.-D. Tsai, *Proc. Natl. Acad. Sci. U. S. A.*, 2011, **108**, 16515–16520.
- 27 M. Nelson, W. Humphrey, A. Gursoy, A. Dalke, L. Kalé, R. D. Skeel and K. Schulten, *J. Supercomputing Appl.*, 1996, **10**, 251–268.
- 28 J. C. Phillips, R. Braun, W. Wang, J. Gumbart, E. Tajkhorshid, E. Villa, C. Chipot, R. D. Skeel, L. Kale and K. Schulten, *J. Comput. Chem.*, 2005, **26**, 1781–1802.
- 29 A. D. Jr MacKerell, D. Bashford, M. Bellott, R. L. Jr Dunbrack, J. Evanseck, M. J. Field, S. Fischer, J. Gao, H. Guo, S. Ha, D. Joseph, L. Kuchnir, K. Kuczera, F. T. K. Lau, C. Mattos, S. Michnick, T. Ngo, D. T. Nguyen, B. Prodhom, I. W. E. Reiher, B. Roux, M. Schlenkrich, J. Smith, R. Stote, J. Straub, M. Watanabe, J. Wiorcikiewicz-Kuczera, D. Yin and M. Karplus, *J. Phys. Chem. B*, 1998, **102**, 3586–3616.
- 30 A. D. Jr Mackerell, M. Feig and C. L. Brooks, *J. Comput. Chem.*, 2004, **25**, 1400–1415.
- 31 H. E. Berman, J. Westbrook, Z. Feng, G. Gilliland, T. N. Bhat, H. Weissig, I. N. Shindyalov and P. E. Bourne, *Nucl. Acids Res.*, 2000, **28**, 235–242.
- 32 F. Gräter, J. Shen, H. Jiang, M. Gautel and H. Grubmüller, *Biophys. J.*, 2005, **88**, 790–804.
- 33 A. D. Humphrey and K. Schulten, *J. Mol. Graphics*, 1996, **14**, 33–38.
- 34 W. L. Jorgensen, J. Chandrasekhar, J. D. Madura, R. W. Impey and M. L. Klein, *J. Chem. Phys.*, 1983, **79**, 926–935.
- 35 H. Grubmüller and V. Groll, SOLVATE 1.0, 1996, <http://www.mpibpc.mpg.de/home/grubmueller/downloads/solvate/index.html>.
- 36 I. Balabin, Meadionize plugin 1.2, 2006, <http://www.chem.duke.edu/~ilya/Software/Meadionize/docs/meadionize.html>.
- 37 D. Bashford, An object-oriented programming suite for electrostatic effects in biological molecules. An experience report on the MEAD project, in *Scientific Computing in Object-Oriented Parallel Environments*, Springer, Berlin, 1997, pp. 233–240.
- 38 E. von Castelmur, J. Strümpfer, B. Franke, J. Bogomolovas, S. Barbieri, H. Qadota, P. V. Konarev, D. I. Svergun, S. Labeit, G. M. Benian, K. Schulten and O. Mayans, *Proc. Natl. Acad. Sci. U. S. A.*, 2012, **109**, 13608–13613.
- 39 R. N. Mantegna and H. E. Stanley, *Nature*, 1995, **376**, 46–49.
- 40 V. Plerou, P. Gopikrishnan and H. E. Stanley, *Nature*, 2003, **421**, 130.
- 41 R. N. Mantegna and H. E. Stanley, *An introduction to econophysics, correlations and complexity in finance*, Cambridge University Press, 2000.
- 42 M.-C. Wu, M.-C. Huang, H.-C. Yu and T. C. Chiang, *Phys. Rev. E: Stat., Nonlinear, Soft Matter Phys.*, 2006, **73**, 016118.
- 43 C.-K. Peng, S. V. Buldyrev, S. Havlin, M. Simons, H. E. Stanley and A. L. Goldberger, *Phys. Rev. E: Stat. Phys., Plasmas, Fluids, Relat. Interdiscip. Top.*, 1994, **49**, 1685–1689.
- 44 H. E. Huang, Z. Shen, S. R. Long, M. C. Wu, H. H. Shih, Z. Zheng, N. C. Yen, C. C. Tung and H. H. Liu, *Proc. R. Soc. London, Ser. A*, 1998, **454**, 903–995.
- 45 M.-C. Wu and C.-K. Hu, *Phys. Rev. E: Stat., Nonlinear, Soft Matter Phys.*, 2006, **73**, 051917.
- 46 M.-C. Wu, *Physica A*, 2007, **375**, 633–642.
- 47 M.-C. Wu, *J. Korean Phys. Soc.*, 2007, **50**, 304–312.
- 48 M.-C. Wu, E. Watanabe, Z. R. Struzik, C.-K. Hu and Y. Yamamoto, *Phys. Rev. E: Stat., Nonlinear, Soft Matter Phys.*, 2009, **80**, 051917.
- 49 M.-C. Wu, *EPL*, 2012, **97**, 48009.
- 50 Z. Wu and N. E. Huang, *Adv. Adapt. Data. Anal.*, 2009, **1**, 1–41.
- 51 T. E. Creighton, *Proteins: Structures and Molecular Properties*, H. E. Freeman and Company, 1993, 2nd edn.
- 52 D. J. Gardiner, *Practical Raman spectroscopy*, Springer-Verlag, 1989.
- 53 X. Li, P. Romero, M. Rani, A. K. Dunker and Z. Obradovic, *Genome Inf.*, 1999, **10**, 30–40.
- 54 P. Romero, Z. Obradovic, X. Li, E. Garner, C. Brown and A. K. Dunker, *Proteins: Struct., Funct., Genet.*, 2001, **42**, 38–48.
- 55 P. Romero, Z. Obradovic and A. K. Dunker, *Genome Inf.*, 1997, **8**, 110–124.

Electronic Supplementary Information for

Correlated vibrations in ion-pair dynamics in mechanoactivation identifies functional domains of force-dependent titin kinase

by Ming-Chya Wu, Jeffrey G. Forbes, and Kuan Wang

Here the same analysis as the main text on more realizations with the same and different pulling speeds are summarized.

I. SUMMARY OF THE SECOND REALIZATION WITH PULLING SPEED $v = 0.005$ Å/PS

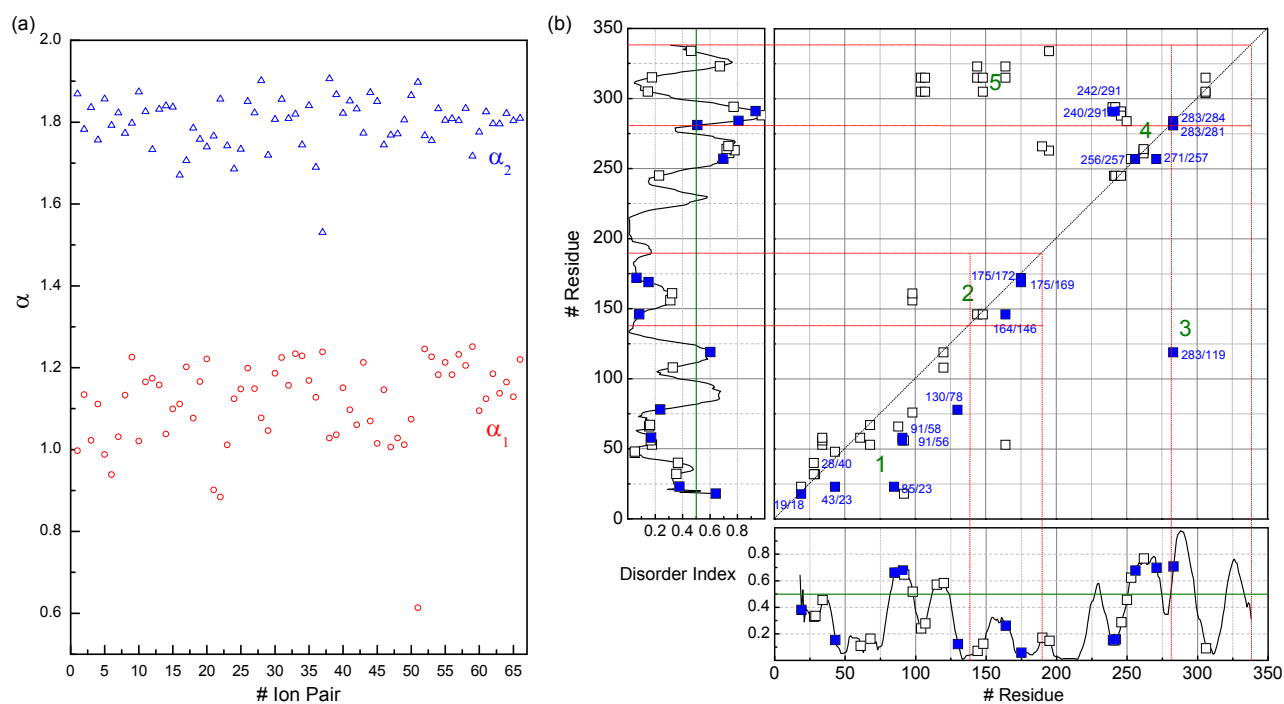


FIG. 1 (a) Distribution of the scaling index α of the 66 ion-pair time series. $\langle \alpha_1 \rangle = 1.11$ and $\langle \alpha_2 \rangle = 1.80$. (b) Diagonal map of all ion pairs (\square) and those with regular oscillatory behaviors in their time series (\blacksquare).

TABLE I Classification of ion pairs. Groups 1, 2, ... 5 are classified by topological locations in linear sequence and their subgroups (I, I*, ...) are classified by the existence of explicit oscillation. Salt-bridges in unstretched protein are underlined. Salt-bridges formed during stretch are without underline. The ion-pair time series having explicit oscillatory behaviors are further highlighted by bold fonts.

| Group | Subgroup | Ion pairs |
|-------|----------|---|
| 1 | I* | E019-K018, E043-K023, E085-K023, E091-K058, E130-R078 |
| | I | <u>D029-R032</u> , <u>E088-K066</u> , E019-K023, E028-R032, E028-R040, E034-K053, E034-K056, E034-K058, E043-K048, D061-K058, E068-K053, E068-K067, E091-K056, E092-K018, E092-K056, E098-R076, E120-R108, E120-R119, E164-K053 |
| 2 | II* | E164-R146, D175-R169, D175-K172 |
| | II | <u>E098-K161</u> , E098-R156, D144-R146, E148-R146 |
| 3 | III* | E283-R119 |
| 4 | IV* | D240-R291, E242-R291, D256-R257, E271-R257, E283-K281, E283-R284 |
| | IV | E190-R266, D195-R263, D240-K294, E241-K245, E242-K245, E242-K294, E246-K245, E246-K288, E246-R291, E250-R284, D253-R257, E262-K261, E262-R263, E262-K264, D306-K304, D306-K305, D306-R315 |
| 5 | V | D104-K305, D104-R315, E107-K305, E107-R315, D144-R315, D144-R323, E148-K305, E148-R315, E164-R315, E164-R323, D195-K334 |

II. SUMMARY OF THE FIRST REALIZATION WITH PULLING SPEED $v = 0.01 \text{ \AA/PS}$

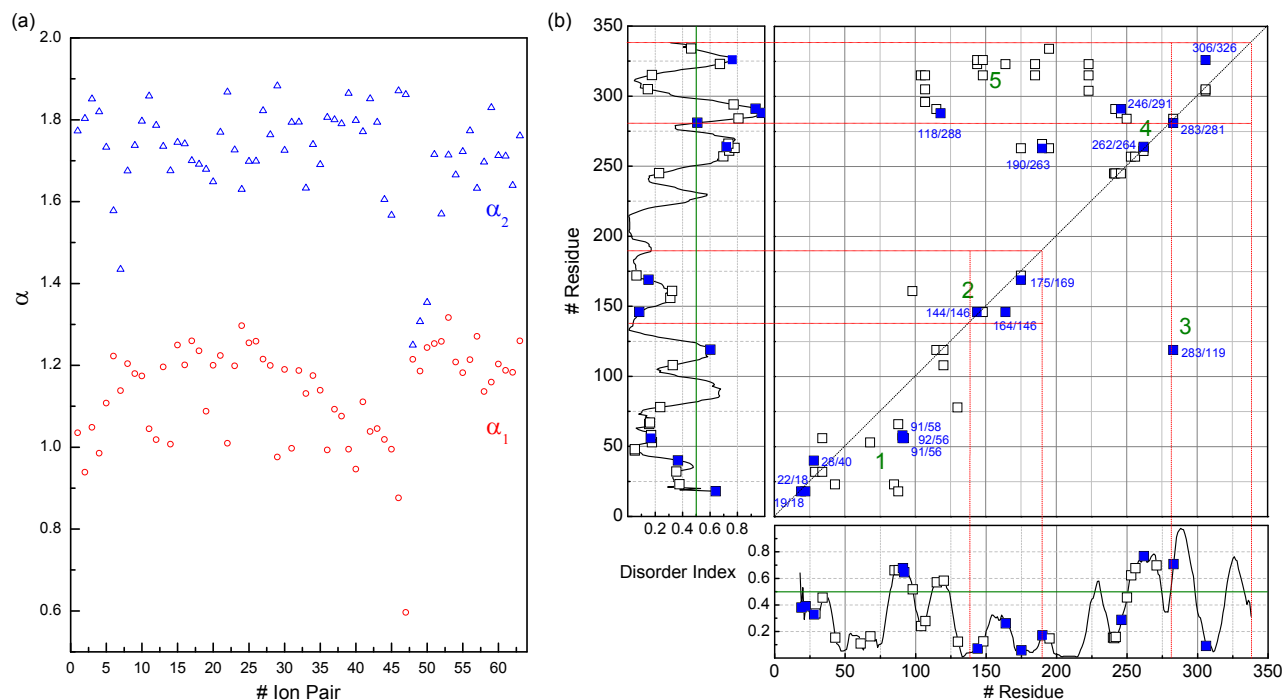


FIG. 2 (a) Distribution of the scaling index α of the 63 ion-pair time series. $\langle \alpha_1 \rangle = 1.13$ and $\langle \alpha_2 \rangle = 1.72$. (b) Diagonal map of all ion pairs (\square) and those with regular oscillatory behaviors in their time series (\blacksquare).

TABLE II Classification of ion pairs. Groups 1, 2, ... 5 are classified by topological locations in linear sequence and their subgroups (I, I*, ...) are classified by the existence of explicit oscillation. Salt-bridges in unstretched protein are underlined. Salt-bridges formed during stretch are without underline. The ion-pair time series having explicit oscillatory behaviors are further highlighted by bold fonts.

| Group | Subgroup | Ion pairs |
|-------|----------|---|
| 1 | I* | <u>E022-K018</u>, <u>E091-K058</u>, <u>E019-K018</u>, <u>E028-R040</u>, <u>E091-K056</u>, <u>E092-K056</u> |
| | I | D029-R032, E034-R032, E034-K056, E043-K023, E068-K053, E085-K023, E088-K018, E088-K066, E115-R119, E120-R108, E120-R119, E130-R078 |
| 2 | II* | <u>D144-R146</u>, <u>E164-R146</u>, <u>D175-R169</u> |
| | II | <u>E098-K161</u> , E148-R146, D175-K172 |
| 3 | III* | <u>E283-R119</u> |
| 4 | IV* | <u>E190-R263</u>, <u>E246-R291</u>, <u>E262-K264</u>, <u>E283-K281</u>, <u>D306-K326</u> |
| | IV | <u>E246-K288</u> , D175-R263, E190-R266, D195-R263, E223-K304, E223-R315, E223-R323, E241-K245, E242-K245, E242-R291, E246-K245, E250-R284, D253-R257, D256-R257, E262-K261, E262-R263, E283-R284, D306-K304, D306-K305 |
| 5 | V* | <u>E118-K288</u> |
| 5 | V | <u>E107-K305</u> , D104-R315, E107-R296, E107-R315, E115-R291, D144-R323, D144-K326, E148-R315, E148-K326, E164-R323, E185-R315, E185-R323, D195-K334 |

III. SUMMARY OF THE SECOND REALIZATION WITH PULLING SPEED $v = 0.01 \text{ \AA/PS}$

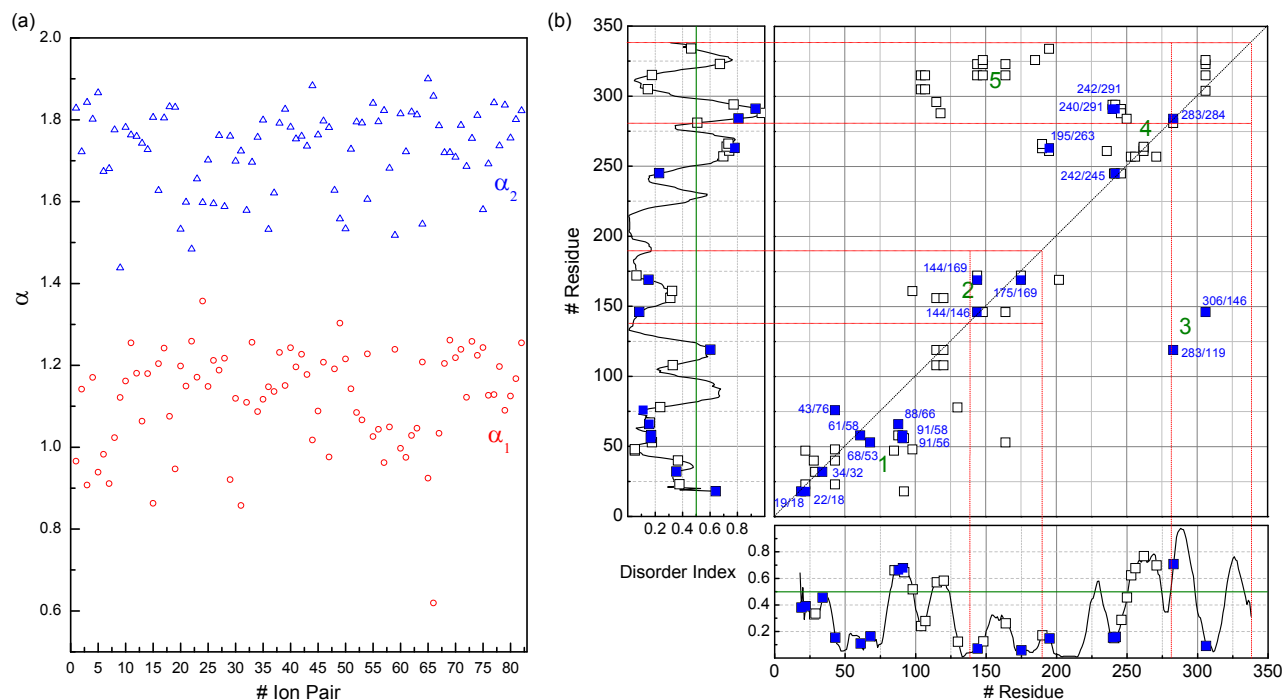


FIG. 3 (a) Distribution of the scaling index α of the 63 ion-pair time series. $\langle \alpha_1 \rangle = 1.12$ and $\langle \alpha_2 \rangle = 1.73$. (b) Diagonal map of all ion pairs (\square) and those with regular oscillatory behaviors in their time series (\blacksquare).

TABLE III Classification of ion pairs. Groups 1, 2, ... 5 are classified by topological locations in linear sequence and their subgroups (I, I*, ...) are classified by the existence of explicit oscillation. Salt-bridges in unstretched protein are underlined. Salt-bridges formed during stretch are without underline. The ion-pair time series having explicit oscillatory behaviors are further highlighted by bold fonts.

| Group | Subgroup | Ion pairs |
|-------|----------|---|
| 1 | I* | E019-K018, E022-K018, E034-R032, E043-R076, D061-K058, E068-K053, E088-K066, E091-K056, E091-K058 |
| | I | <u>E022-K023, E022-K047, E028-R040, D029-R032, E043-K023, E043-R040, E043-K048, E085-K047, E088-K058, E092-K018, E092-K056, E098-K048, E115-R108, E115-R119, E120-R108, E120-R119, E130-R078, E164-K053</u> |
| 2 | II* | D144-R146, D144-R169, D175-R169 |
| | II | <u>E098-K161, E115-R156, E120-R156, D144-K172, E148-R146, E164-R146, D175-K172</u> |
| 3 | III* | E283-R119, D306-R146 |
| 4 | IV* | D195-R263, D240-R291, E242-R291, E242-K245, E283-R284 |
| | IV | <u>E283-K281, E190-R263, E190-R266, D195-K261, D195-K334, D202-R169, E236-K261, D240-K294, E241-K245, E242-K294, E246-K245, E246-K288, E246-R291, E250-R284, D253-R257, D256-R257, E262-K261, E262-R263, E262-K264, E271-R257, D306-K304, D306-R315, D306-R323, D306-K326</u> |
| 5 | V | <u>D104-K305, D104-R315, E107-K305, E107-R315, E115-R296, E118-K288, D144-R315, D144-R323, E148-R315, E148-R323, E148-K326, E164-R315, E164-R323, E185-K326</u> |

IV. SUMMARY OF THE REALIZATION WITH PULLING SPEED $v = 0.05 \text{ \AA/PS}$

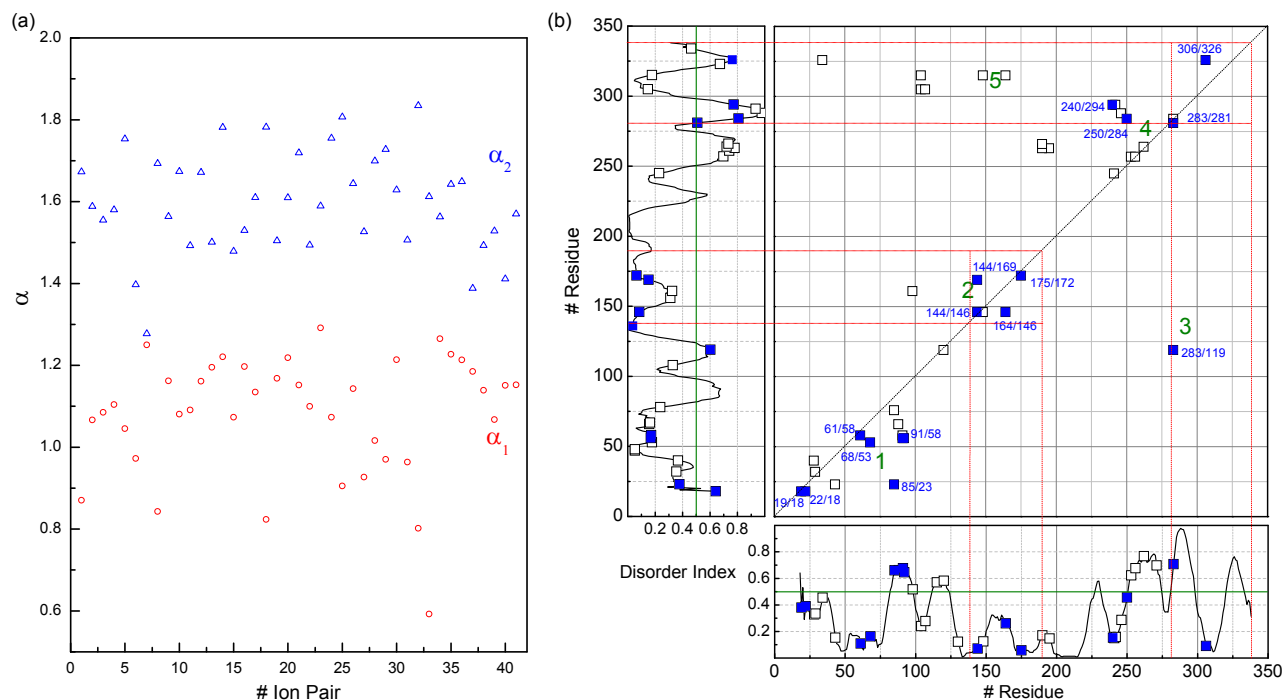


FIG. 4 (a) Distribution of the scaling index α of the 63 ion-pair time series. $\langle \alpha_1 \rangle = 1.08$ and $\langle \alpha_2 \rangle = 1.60$. (b) Diagonal map of all ion pairs (\square) and those with regular oscillatory behaviors in their time series (\blacksquare).

TABLE IV Classification of ion pairs. Groups 1, 2, ... 5 are classified by topological locations in linear sequence and their subgroups (I, I*, ...) are classified by the existence of explicit oscillation. Salt-bridges in unstretched protein are underlined. Salt-bridges formed during stretch are without underline. The ion-pair time series having explicit oscillatory behaviors are further highlighted by bold fonts.

| Group | Subgroup | Ion pairs |
|-------|----------|---|
| 1 | I* | <u>E022-K018</u> , <u>E091-K058</u> , <u>E019-K018</u> , <u>D061-K058</u> , <u>E068-K053</u> , <u>E085-K023</u> , <u>E091-K056</u> , <u>E092-K056</u> |
| | I | E028-R040, D029-R032, E043-K023, E085-R076, E088-K066, E120-R119 |
| 2 | II* | D144-R146 , D144-R169 , E164-R146 , D175-K172 |
| | II | <u>E098-K161</u> , E148-R146 |
| 3 | III* | E283-R119 |
| 4 | IV* | D240-K294 , E250-R284 , E283-K281 , D306-K326 |
| | IV | E190-R263, E190-R266, D195-R263, E241-K245, E242-K294, E246-K288, D253-R257, D256-R257, E262-K264, E283-R284 |
| 5 | V | <u>E107-K305</u> , E034-K326, D104-K305, D104-R315, E148-R315, E164-R315 |